Mon. Not. R. astr. Soc. (1988) **234,** *Short Communication,* 5P–18P

Spectroscopic and photometric observations of SN 1987A–IV. Days 260–385

P. A. Whitelock[1], R. M. Catchpole[1], J. W. Menzies[1], M. W. Feast[1], H. Winkler[2], F. Marang[1], I. S. Glass[1], L. A. Balona[1], J. Egan[1], B. S. Carter[1], G. Roberts[1], K. Sekiguchi[1], C. D. Laney[1], T. Lloyd Evans[1], J. D. Laing[1], J. Spencer Jones[1], J. Fernley[3], P. James[4], A. P. Fairall[2], A. S. Monk[5] and F. van Wyk[1]

[1] *South African Astronomical Observatory, PO Box 9, Observatory 7935, South Africa*
[2] *University of Cape Town, Private Bag, Rondebosch, 7700, South Africa*
[3] *University College London, Gower Street, London WC1E 6BT*
[4] *Imperial College, Blackett Laboratory, London SW7 2BZ*
[5] *Royal Greenwich Observatory, Herstmonceux Castle, Hailsham, Sussex*

Accepted 1988 May 9. Received 1988 May 9; in original form 1988 April 6

Summary. Spectroscopic and photometric $[UBV(RI)_cJHKLM]$ observations of SN 1987A in the Large Magellanic Cloud are described and briefly discussed. These cover the interval from days 260–385 after core collapse. During this period the bolometric light curve, determined from optical and infrared photometry, has been declining slightly faster than the rate expected for the radioactive decay of ^{56}Co. The flux deficit is, however, compensated for by γ-radiation, indicating that the decay of ^{56}Co continues to be the sole significant energy source for the supernova.

1 Introduction

Spectroscopic and photometric observations of SN 1987A for the first 259 days after its discovery were presented by Menzies *et al.* (1987) and Catchpole *et al.* (1987, 1988), hereafter Papers I, II and III. In the present paper data for the interval from days 260 to 385 are discussed. As in Papers II and III the Kamiokonde-II neutrino event is adopted as the epoch of the supernova outburst (JD 2446849.816, 1987 February 23.316), and A_v=0.6 mag is taken to be the extinction. Intense theoretical and observational interest in SN 1987A continues; at this stage concern is particularly centred on the energy balance and on evidence of material which has undergone nuclear processing within the supernova.

2 Spectroscopy

2.1 OPTICAL OBSERVATIONS

The spectral coverage of the supernova has continued at a rate of about one spectrum per 10 days. Spectra were recorded with an intensified Reticon detector attached to the Grating spectrograph at the Cassegrain focus of the 1.9-m telescope at Sutherland. With a 300 line mm^{-1} grating used in the first order the resolution is about 7 Å (FWHM) over the wavelength range from 3400 to 7600 Å. The limited dynamic range of the detector has forced us to obtain two spectra per night through different neutral density filters to record both the Hα line and the continuum adequately.

Table 1. SN 1987A. Dates on which spectra were obtained. HJD-2440000.

7110.42	7121.59	7158.34	7187.99	7219.51
7112.55	7127.47	7158.37	7187.99	7219.53
7112.57	7127.50	7165.32	7194.33	7231.45
7115.46	7137.33	7165.34	7194.35	7231.47
7115.48	7137.36	7172.34	7201.32	7233.38
7116.41	7145.34	7172.37	7204.33	7233.40
7116.43	7145.36	7180.38	7204.36	
7118.58	7150.32	7180.40	7212.26	
7121.57	7150.34	7180.43	7212.28	

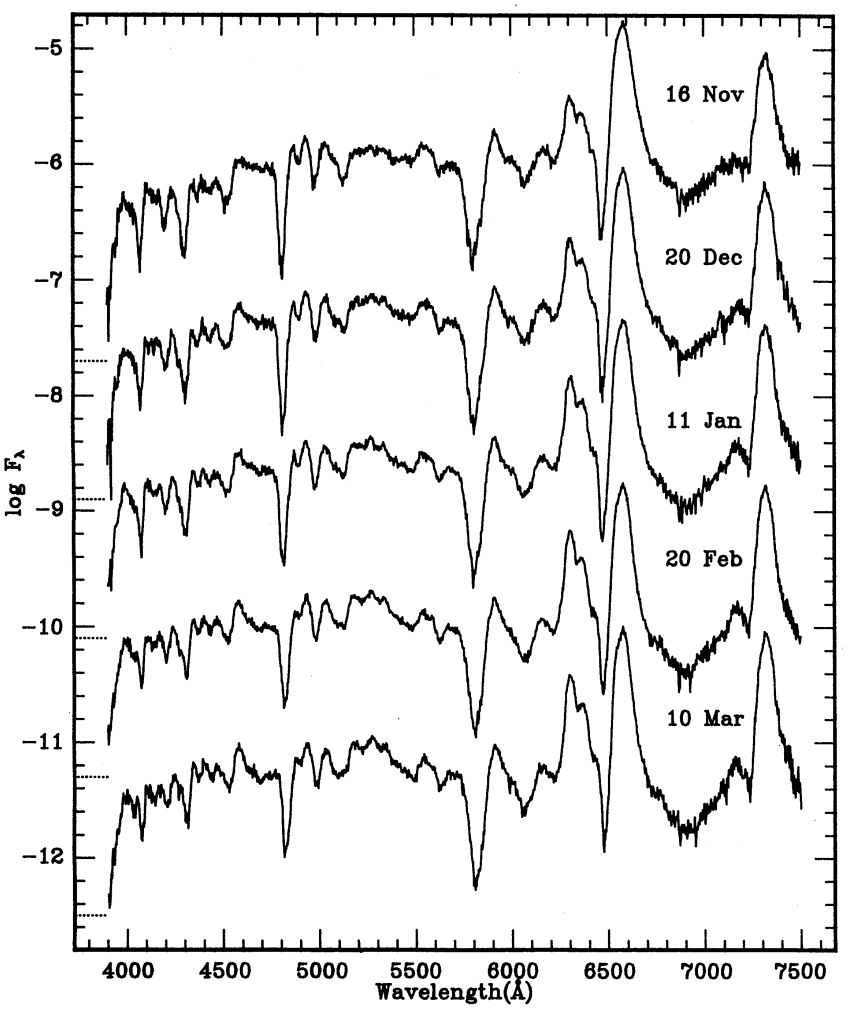

Figure 1. Spectra of SN 1987A. Log flux (erg cm^{-2} s^{-1} $Å^{-1}$) is plotted against wavelength (Å). The dotted lines on the left side indicate the level of log $F_\lambda = -12.5$ for successive spectra.

Each spectrum was reduced to flux units by comparison with a standard star observed on the same night. To put the fluxes on to an absolute scale they were multiplied by an appropriate factor to give agreement between the V magnitude calculated from the spectrum and that obtained photoelectrically. The log of observations is given in Table 1.

Selected spectra are shown in Fig. 1, where for convenience of display it has been necessary to plot log flux on the vertical axis and only the range from 3900 to 7500 Å. The main change in the spectrum in this period has been the growth in prominence of the [O I] lines at 6300 and 6364 Å. The Hα line remains the dominant feature, though the [Ca II] 7291/7324 Å blend has about the same peak flux as Hα in the later spectra. Between 1987 November and 1988 March the total flux in the Hα emission line declined by about a factor of 3, while that in the [O I] lines increased by about 30 per cent and that in the [Ca II] lines declined by 30 per cent. These results depend to some extent on the definition of the continuum level and we have attempted to measure the fluxes in a consistent way in the different spectra.

2.2 INFRARED OBSERVATIONS (1.1–4.0 μm)

The spectra shown in Fig. 2 were obtained on 1987 December 4, 1988 January 4 and March 14 (days 285, 316, 385) using the SAAO filterwheel spectrometer, at a resolution ($\lambda/\delta\lambda$) of about 100, mounted at the Cassegrain focus of the 1.9-m telescope. They were reduced as described in Paper III.

The spectrum shown in Fig. 3 was obtained with a new grating spectrometer used in conjunc-

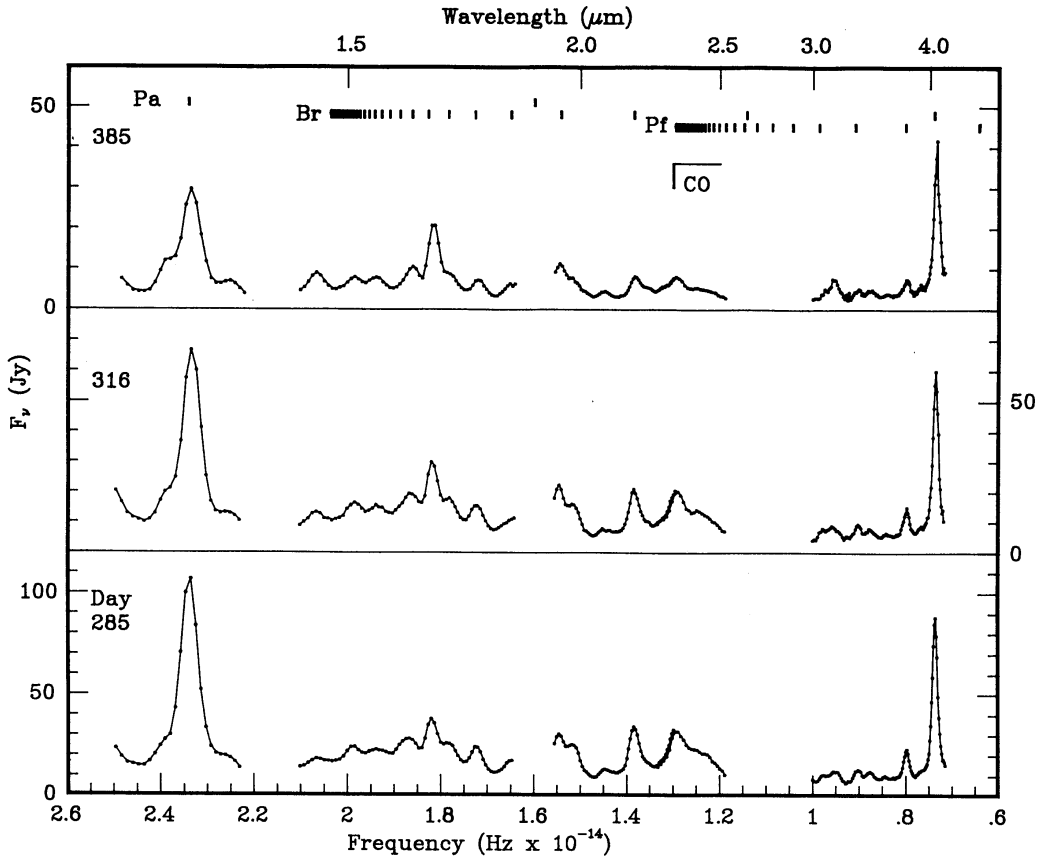

Figure 2. The infrared spectra obtained on days 285, 316 and 385. Note that the scales are all different. In the top panel the three rows of short vertical ticks mark the postions of the lines in the Paschen, Brackett and Pfund series, respectively. The position of the CO first overtone vibration–rotation band is also indicated.

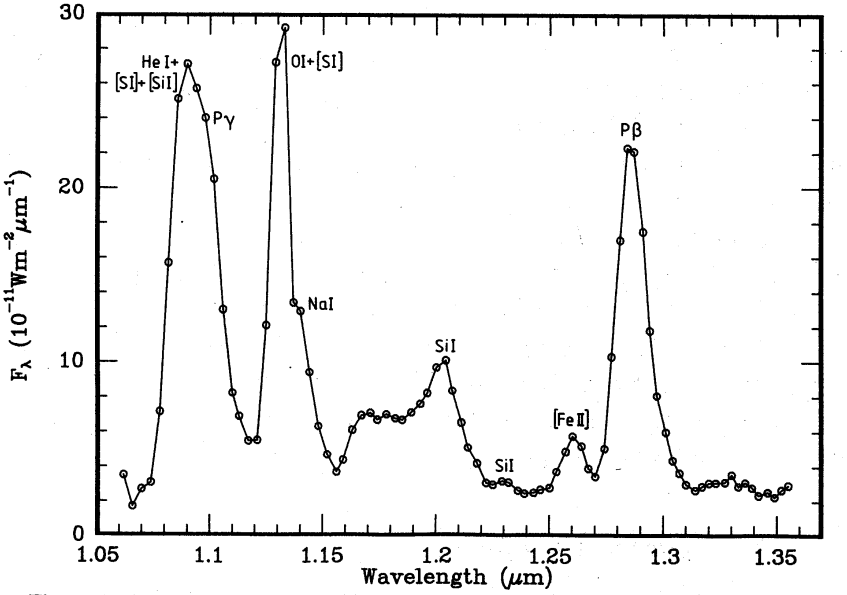

Figure 3. A spectrum of SN 1987A taken on day 289 and covering the *J*-band.

tion with the Mk III IR photometer on the 1.9-m telescope. The resolution ($\lambda/\delta\lambda$) is about 500 and more details of the instrument will be given by Glass (in preparation). The absolute calibration was made with respect to Sirius and is probably good to between 15 and 20 per cent.

The features in the Fig. 3 spectrum have been identified using the line list published by Oliva, Moorwood & Danziger (1988) and are marked on Fig. 3. Comparing the spectra in Fig. 2 with those of Paper III (fig. 2) it is apparent that the features are, at least superficially, very similar. There is no longer any clearly defined continuum as lines blend one with another. The Brackett γ and Paschen β intensities have fallen more rapidly than has the bolometric flux, while the Brackett α to Paschen β flux ratio has gradually increased reaching 0.46, the case B value, by day 385. The feature at 1.64 μm, probably a blend of [Si I] and [Fe II], with Brackett 12, has become much more prominent. It is not clear from these low resolution spectra exactly what the features between 2.3 and 2.6 μm are. At earlier epochs (Paper III) emission from the CO first overtone dominated this region. If this is still the case then the shape of the band suggests a continuation of the trend to lower temperatures. A comparison with theoretical CO band intensities (Young 1968) would indicate that by early 1988 (day 316) a significant fraction of the CO was at temperatures below 1000 K. An alternative explanation of the features in this region is that the CO band is extremely weak and that the feature at 2.32 μm has some other origin. One possible identification would be the Ar II line at 2.313 μm ($4d^4F_{9/2}$–$5p\,4D^0_{7/2}$), although as this line is of high excitation, some sort of resonance flourescence mechanism might be required. Argon is expected to be over-abundant in material that has undergone explosive oxygen or silicon burning (Woosley, Arnett & Clayton 1973) and its detection in late 1987 would be consistent with other observational evidence (e.g. the presence of γ-radiation and the change in the decline rate of the bolometric light curve; see Section 8) that processed material has penetrated into the envelope. Rank *et al.* (1988) have identified Ar II lines as well as Ni I, Ni II and Co II in a spectrum of SN 1987A taken during 1987 November and covering the 4–12 μm spectral range.

3 Photometry

3.1 OPTICAL DATA (0.35–0.8 μm)

The $UBV(RI)_c$ data are listed in Table 2. These were obtained with the same telescope, photometer, etc., as the measurements reported in Papers I–III. As previously, the zero point

Table 2. $UBV(RI)_c$ photometry of SN 1987A.

JD 2446800+	V	(B-V)	(U-B)	(V-R)	(V-I)
310.350	5.660	1.358	1.672	1.144	1.700
313.287	5.692	1.357	1.639	1.140	1.693
313.572	5.675	1.365	1.639	1.139	1.674
314.293	5.690	1.369	1.632	1.152	1.691
314.598	5.687	1.368	1.650	1.144	1.679
315.374	5.71	1.35	1.63	1.14	1.70
316.333	5.72	1.35	1.62	1.15	1.70
318.430	5.732	1.342	1.627	1.144	1.684
319.269	5.73	1.35	1.60	1.16	1.69
320.386	5.757	1.341	1.599	1.156	1.707
321.471	5.761	1.338	1.601	1.145	1.689
322.458	5.768	1.349	1.578	1.150	1.686
323.295	5.786	1.330	1.606	1.170	1.701
323.472	5.786	1.323	1.590	1.157	1.696
324.323	5.788	1.331	1.571	1.144	1.691
324.516	5.796	1.323	1.569	1.143	1.690
325.360	5.802	1.324	1.570	1.147	1.688
326.452	5.818	1.321	1.563	1.154	1.680
327.394	5.823	1.322	1.557	1.144	1.690
327.492	5.824	1.316	1.554	1.142	1.690
329.343	5.84	1.31	1.54	1.15	1.70
329.496	5.84	1.31	1.54	1.14	1.69
331.375	5.855	1.307	1.529	1.142	1.693
332.479	5.871	1.299	1.527	1.148	1.690
333.423	5.877	1.299	1.529	1.144	1.700
335.430	5.895	1.291	1.517	1.146	1.687
336.390	5.910	1.297	1.510	1.153	1.681
338.459	5.930	1.284	1.493	1.152	1.689
341.345	5.952	1.280	1.473	1.140	1.680
341.356	5.950	1.272	1.484	1.150	1.675
342.393	5.97	1.27	1.46	1.15	1.69
343.347	5.970	1.271	1.463	1.142	1.681
344.361	5.984	1.267	1.456	1.146	1.680
344.483	5.985	1.269	1.463	1.144	1.681
345.279	5.985	1.261	1.421	1.146	1.677
347.333	6.000	1.262	1.449	1.144	1.687
348.287	6.004	1.262	1.421	1.141	1.676
349.364	6.029	1.257	1.427	1.148	1.682
352.337	6.06	1.24	1.42	1.14	1.68
352.436	6.05	1.24	1.43	1.13	1.66
353.431	6.065	1.245	1.412	1.137	1.666
354.514	6.07	1.25	1.40	1.14	1.66
355.441	6.089	1.239	1.395	1.143	1.669
356.325	6.10	1.24	1.40	1.14	1.66
357.335	6.107	1.234	1.393	1.132	1.664
358.306	6.11	1.23	1.38	1.14	1.66
359.337	6.12	1.23	1.39	1.14	1.66
360.378	6.130	1.231	1.370	1.135	1.656
362.582	6.146	1.218	1.357	1.152	1.656
363.376	6.16	1.22	1.35	1.14	1.66
364.399	6.165	1.212	1.357	1.137	1.651
365.392	6.18	1.21	1.35	1.14	1.64
366.399	6.184	1.211	1.349	1.135	1.643
367.445	6.198	1.200	1.353	1.149	1.635
368.373	6.203	1.207	1.339	1.130	1.643
369.495	6.210	1.200	1.340	1.134	1.641
370.314	6.227	1.195	1.337	1.132	1.643
371.290	6.227	1.192	1.327	1.133	1.645
372.401	6.238	1.191	1.318	1.143	1.646
373.383	6.257	1.184	1.311	1.138	1.641
374.404	6.269	1.180	1.310	1.138	1.637
375.397	6.277	1.185	1.300	1.135	1.626
376.297	6.280	1.188	1.298	1.124	1.626
377.323	6.293	1.180	1.296	1.125	1.624
378.377	6.302	1.183	1.303	1.128	1.630
382.446	6.343	1.168	1.288	1.114	1.617
383.457	6.348	1.163	1.275	1.127	1.616
385.469	6.373	1.158	1.267	1.123	1.616
386.464	6.379	1.163	1.260	1.123	1.612
387.323	6.385	1.155	1.242	1.116	1.601
388.314	6.398	1.151	1.236	1.116	1.593
389.314	6.407	1.147	1.232	1.108	1.595
391.294	6.420	1.144	1.224	1.109	1.591
392.370	6.437	1.137	1.217	1.118	1.602
393.327	6.441	1.136	1.224	1.107	1.589
394.288	6.455	1.137	1.200	1.111	1.585
395.304	6.463	1.131	1.218	1.114	1.581
396.290	6.471	1.127	1.199	1.104	1.575
398.444	6.493	1.113	1.190	1.104	1.563
401.455	6.523	1.108	1.180	1.091	1.563
402.443	6.532	1.103	1.172	1.105	1.570
403.437	6.533	1.109	1.166	1.097	1.554
404.366	6.549	1.110	1.171	1.099	1.560
405.411	6.58	1.10	1.17	1.10	1.55
409.396	6.59	1.10	1.14	1.08	1.55
412.266	6.624	1.090	1.137	1.088	1.537
413.266	6.624	1.108	1.130	1.074	1.525
414.268	6.636	1.094	1.132	1.063	1.524
415.300	6.66	1.07	1.13	1.08	1.53
417.309	6.67	1.08	1.13	1.07	1.52
419.320	6.683	1.071	1.115	1.068	1.508
419.339	6.692	1.076	1.094	1.069	1.512
420.317	6.707	1.065	1.096	1.087	1.511
423.307	6.732	1.063	1.075	1.060	1.495
424.309	6.738	1.060	1.068	1.062	1.488
430.274	6.83	1.01	1.08	1.07	1.50
433.288	6.828	1.037	1.064	1.040	1.472
435.279	6.849	1.033	1.052	1.049	1.470

Table 3. *JHKL* photometry of SN 1987A.

JD 2446800+	J	H	K	L
310.39	3.83	3.92	3.43	3.10
313.52	3.874	3.968	3.458	3.202
314.30	3.876	3.976	3.500	3.221
314.55	3.880	3.983	3.499	3.222
315.38	3.88	3.99	3.50	3.25
316.36	3.896	4.008	3.529	3.245
317.30	3.911	4.001	3.530	3.269
318.43	3.924	4.037	3.549	3.283
319.34	3.946	4.043	3.576	3.321
320.36	3.946	4.059	3.590	3.318
321.31	3.966	4.068	3.603	3.333
322.37	3.979	4.083	3.623	3.346
323.41	4.007	4.100	3.643	3.362
324.44	3.998	4.119	3.641	3.386
325.51	4.013	4.126	3.682	3.387
326.47	4.019	4.124	3.674	3.395
327.48	4.049	4.150	3.701	3.417
329.38	4.08	4.18	3.73	3.49
331.34	4.101	4.211	3.767	3.505
332.39	4.124	4.223	3.795	3.485
333.40	4.110	4.222	3.797	3.505
334.38	4.120	4.238	3.814	3.524
335.40	4.151	4.262	3.846	3.541
336.40	4.159	4.284	3.860	3.566
338.46	4.176	4.293	3.890	3.568
341.47	4.222	4.330	3.929	3.55
343.39	4.249	4.352	3.961	3.652
344.38	4.261	4.368	3.989	3.653
345.49	4.29	4.39	4.00	3.68
347.36	4.298	4.424	4.020	3.723
348.41	4.325	4.428	4.039	3.748
349.40	4.329	4.438	4.063	3.735
350.39	4.334	4.451	4.065	3.772
352.33	4.357	4.470	4.096	3.771
353.28	4.376	4.475	4.119	3.781
354.51	4.389	4.504	4.139	3.785
355.28	4.402	4.533	4.144	3.791
356.27	4.425	4.526	4.169	3.851
357.27	4.429	4.540	4.189	3.857
358.32	4.45	4.56	4.21	3.87
359.33	4.465	4.562	4.223	3.873
360.38	4.474	4.576	4.235	3.909
361.32	4.487	4.593	4.237	3.894
362.58	4.52	4.61	4.27	3.99
363.32	4.514	4.609	4.271	3.929
364.39	4.517	4.620	4.291	3.932
365.38	4.537	4.629	4.305	3.963
369.34	4.589	4.692	4.363	3.987
370.41	4.601	4.683	4.385	4.039
371.32	4.63	4.71	4.43	4.09
372.31	4.615	4.730	4.408	4.018
373.30	4.642	4.728	4.443	4.098
374.42	4.643	4.731	4.457	4.104
375.44	4.647	4.730	4.461	4.095
376.36	4.655	4.755	4.483	4.111
377.36	4.688	4.773	4.499	4.091
378.36	4.684	4.773	4.493	4.108
382.35	4.748	4.825	4.577	4.189
383.33	4.751	4.832	4.581	4.165
385.33	4.778	4.864	4.608	4.185
386.38	4.801	4.868	4.618	4.234
387.29	4.830	4.882	4.660	4.208
388.33	4.814	4.898	4.663	4.272
389.30	4.835	4.895	4.677	4.271
390.36	4.87	4.92	4.69	
391.33	4.892	4.944	4.729	4.348
392.37	4.872	4.940	4.731	4.273
393.34	4.867	4.938	4.725	4.301
394.31	4.901	4.968	4.771	4.301
395.29	4.924	4.969	4.772	4.325
396.29	4.92	4.98	4.79	
398.46	4.97	5.02	4.86	
399.59	4.940	4.991	4.829	4.359
401.48	4.958	5.020	4.872	4.386
402.60	4.982	5.009	4.875	4.333
403.60	5.018	5.042	4.881	4.473
404.29	5.014	5.058	4.894	4.421
405.41	5.02	5.06	4.93	
406.57	5.043	5.063	4.937	4.418
409.41	5.086	5.101	4.987	4.484
412.28	5.121	5.150	5.024	4.525
413.26	5.137	5.163	5.041	4.513
414.27	5.155	5.168	5.048	4.522
415.31	5.150	5.165	5.070	4.563
417.32	5.159	5.195	5.098	4.588
418.54	5.181	5.191	5.118	4.576
419.26	5.200	5.216	5.133	4.587
420.27	5.220	5.227	5.148	4.606
423.39	5.238	5.247	5.195	
424.3	5.252	5.253	5.203	4.655
428.51	5.295	5.279	5.264	4.71
430.58	5.32	5.29	5.29	4.77
431.56	5.33	5.30	5.31	4.68
433.31	5.378	5.347	5.345	4.734
435.30	5.394	5.376	5.370	4.766

Table 4. *L*, *L'* and *M* photometry.

JD 2446800+	L	L' (mag)	M	Notes	JD 2446800+	L	L' (mag)	M	Notes
319.41			0.78	0.75	360.45	3.90	3.06	1.24	
320.39			0.78	0.75	363.47	3.92	3.08	1.24	
331.42	3.52	2.72	0.98		390.3	4.27	3.43	1.56	
332.45	3.51	2.78	0.96		391.3	4.25		1.51	
333.48	3.51	2.73	0.98		392.3	4.32		1.61	
334.59	3.54	2.75	0.98		393.3	4.31		1.60	
335.47	3.54	2.80	0.99		395.51	4.33	3.48	1.59	
336.51	3.56	2.78	1.00		399.61	4.38	3.58	1.64	
343.37	3.67	2.86	1.09		413.34			1.84	0.75
353.35			1.17		415.44	4.55	3.71	1.81	
354.59			1.19		423.30	4.65	3.82	1.90	
355.34	3.84	3.04	1.17		424.24	4.63	3.83	1.87	
356.36	3.91	3.11	1.23		428.50	4.70	3.92	1.93	
357.35			1.16		435.29	4.76	4.00	1.99	
359.39	3.89	3.08	1.24						

was defined by observations of the nearby standard CPD−68°375. In order to reduce the intensity to a measurable level a 1.8 mag mask was used until JD 2447200 and a 1.1 mag mask thereafter.

The internal standard errors of the magnitudes and colours in Table 2 should be less than 0.01 mag except for data given to only two significant figures in which case problems were experienced with weather conditions.

3.2 INFRARED DATA (1.2–5 μm)

The *JHKL* photometry obtained with the 0.75-m telescope is listed in Table 3 and as with the data given in our previous papers has been reduced to the nearby standard HR 1953. The internal observational errors in *J*, *H* and *K* are 0.01 mag or less while those at *L* have increased since Paper III due to fading of the supernova but are still less than 0.04 mag.

Table 4 contains a number of observations made at *L*, *L'* and *M*. Measurements were made on three nights with the 0.75-m telescope (as indicated in the notes), while the remainder were made with the 1.9-m. The internal observational errors are less than 0.03, 0.02 and 0.05 for *L*, *L'* and *M*, respectively obtained on the 1.9-m and less than 0.08 for the *M* observations made with the 0.75-m telescope.

4 *M* (4.8 μm) excess

The very strong flux in the *M* band is due primarily to emission in the CO fundamental vibration–rotation band (Paper III). The temporal variation of the *M* magnitude and of its contribution to M_{bol}, represented as $M_{bol}-M$, is shown in Fig. 4. It is clear from this that although the flux in *M* is decreasing, its fractional contribution to the bolometric flux has remained constant since about day 180. During this period of constant $M_{bol}-M$ the flux in the CO first-overtone band at 2.4 μm has decreased relative to that in the *M*-band, and therefore presumably relative to the flux in the CO fundamental. The constancy of $M_{bol}-M$ is probably the result of saturation of the fundamental. When the emission in this band becomes optically thin we would expect $M_{bol}-M$ to decrease as the *M* flux drops precipitously. Reasons for including the *M* point in the bolometric flux calculations were given in Paper III; these continue to apply throughout the period covered by the present discussion.

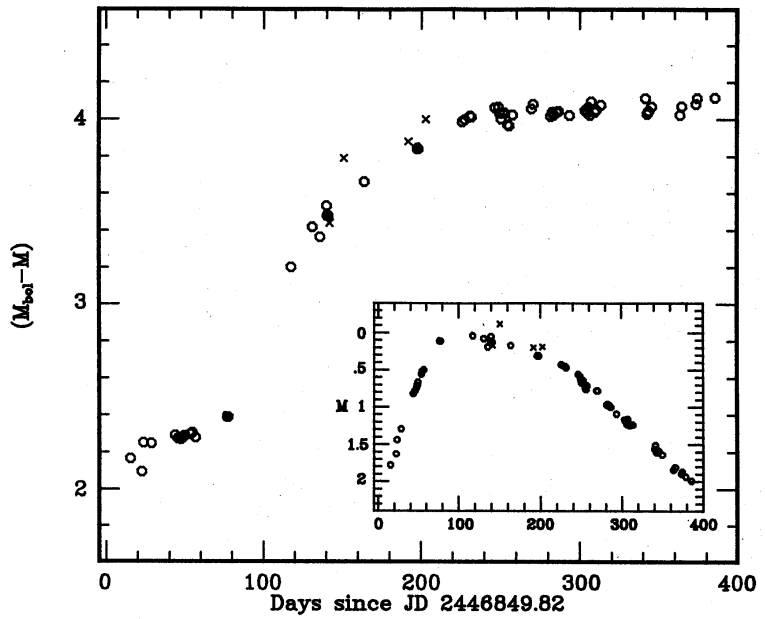

Figure 4. $M_{bol}-M$ is shown as a function of time. The inset shows the variation of M with time. Data obtained with the bolometer are shown as crosses while AAO data are shown as filled symbols (see Paper III).

5 Bolometric light curve

The form of the bolometric flux curve is one of the most important sources of information on the internal energetics of the supernova explosion. A crucial test of any supernova model is its ability to reproduce accurately the observed temporal development of the bolometric flux. It is therefore of equal importance that sources of error and bias in the measured bolometric fluxes be clearly understood.

During the period under discussion here, the continuum in the optical and infrared has faded, and at least half of the bolometric flux is contributed by emission lines. This is illustrated by Fig. 5 which is a composite optical and infrared spectrum on which the coverage of the photometric bands is indicated. Ideally the way to measure the bolometric light curve is to obtain frequent, accurate spectrophotometry over the ultraviolet, optical and infrared spectral regions. In practice it is difficult to do this with the required accuracy (<10 per cent) at any one epoch and almost impossible to do it regularly. The best practical approach seems to be to compare the accurate spectrophotometry obtained from ground-based and space observatories at particular epochs with the more regularly obtained photometry such as that reported here. This approach should provide a good basis for understanding the errors involved in any particular method of measuring bolometric fluxes. In any case the existence of a database of bolometric magnitudes based on broadband photometry should prove extremely useful for comparison with more distant supernovae for which higher resolution measurements may be very difficult to obtain.

The problem with using broadband photometry to determine the bolometric flux is associated with the difficulty of placing photometry of an object with an unusual flux distribution on to a standard photometric system. This was discussed in Paper III and the gradual increase in line equivalent widths which has occurred over recent weeks will undoubtedly have worsened this problem. Nevertheless, it should be possible, using photometry, to establish a reasonable estimate of the total flux, provided that there are no major spectral features outside the range covered by the filters. In the visual the $UBV(RI)_c$ filter response functions overlap and good spectral coverage is achieved. In particular the very strong Hα, [Ca II] and Ca II lines are included within the R_c and I_c bands. The situation in the infrared is not as satisfactory as the photometric

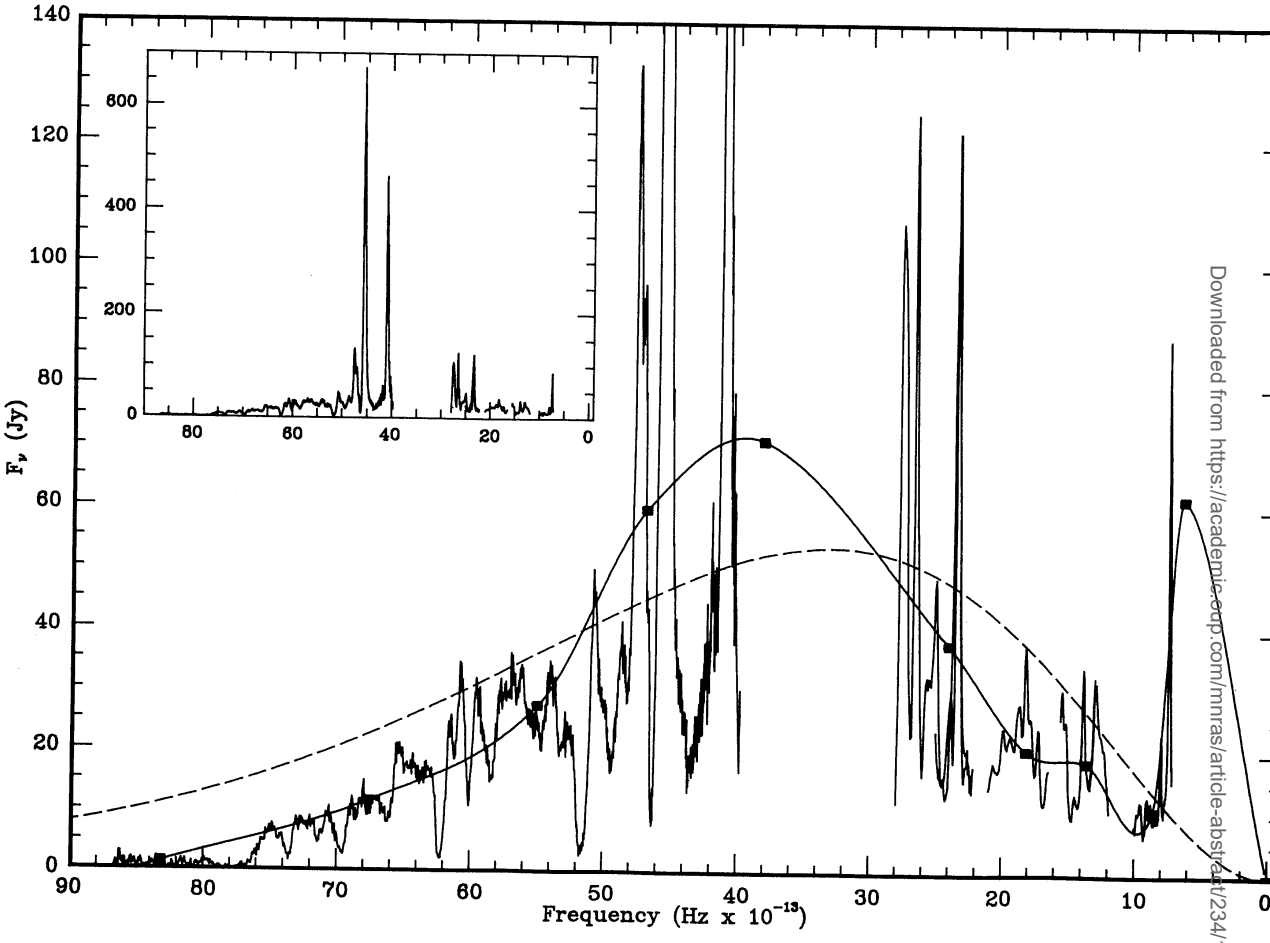

Figure 5. A composite spectrum of the supernova obtained around day 290. The broadband observations are represented as squares. The dashed line shows the blackbody fit and the continuous line the spline fit to these points. The inset shows the strengths of the lines which are off scale on the main figure.

bands are essentially defined by the deep telluric H_2O absorption features and there is necessarily no overlap. In particular, Paschen α which falls between the H and K bands is excluded. We estimate that since the onset of the linear decline the bolometric magnitude will be underestimated by 0.03 mag by this exclusion. Coincidentally, a compensating error of almost exactly the same magnitude is introduced when bolometric fluxes are calculated from spline fits to the U–M data. This is because the flux from the CO fundamental vibration–rotation band which occurs in the M band does not have as broad a distribution in wavelength as is suggested by the spline fit.

Following the procedure described in Paper III we derived the bolometric flux by integration under a smooth curve taken as a representation of the data. Two different curves have been tried, namely, a blackbody curve fitted by least squares to the data points and a spline curve which necessarily goes through all the points and is constrained to go through zero at the ends. In each case, the fits were first made to the data for all bands from U to L and repeated with the M point included. This resulted in four representations of the bolometric light curve. The results are given in Table 5. The luminosity may be calculated from the tabulated bolometric magnitudes using the expression:

$$L = 838 \times 10^{(40 - 0.4 \times m_{bol})} \quad \text{erg s}^{-1},$$

which assumes the distance modulus of SN 1987A is 18.5.

Table 5. Derived data for SN 1987A.

Time	Bolometric Magnitude				Time	Bolometric Magnitude			
	U to L		U to M			U to L		U to M	
Day	bb	spline	bb	spline	Day	bb	spline	bb	spline
260.55	4.72	4.87			313.52	5.25	5.43	5.25	5.32
263.73	4.75	4.90			314.57	5.26	5.43		
264.48	4.75	4.91			315.56	5.28	5.45		
265.55	4.77	4.92			319.58	5.32	5.49		
266.52	4.78	4.93			320.54	5.33	5.51		
268.61	4.80	4.95			321.48	5.33	5.51		
269.48	4.79	4.95	4.78	4.85	322.55	5.33	5.51		
270.55	4.81	4.97	4.80	4.86	323.48	5.36	5.54		
271.58	4.83	4.98			324.59	5.37	5.55		
272.59	4.83	4.99			325.60	5.38	5.56		
273.62	4.85	5.01			326.51	5.39	5.57		
274.56	4.85	5.01			327.52	5.41	5.58		
275.61	4.87	5.03			328.55	5.41	5.59		
276.64	4.88	5.04			332.57	5.46	5.64		
277.67	4.89	5.05			333.57	5.48	5.66		
279.52	4.90	5.07			335.58	5.49	5.67		
281.54	4.92	5.09	4.92	4.99	336.60	5.50	5.68		
282.61	4.94	5.10	4.93	5.00	337.49	5.51	5.69		
283.59	4.94	5.11	4.93	5.00	338.50	5.52	5.70		
285.59	4.97	5.13	4.96	5.03	339.48	5.53	5.72		
286.58	4.98	5.15	4.97	5.04	341.49	5.55	5.74	5.55	5.62
288.64	5.00	5.16			342.55	5.56	5.74	5.55	5.64
291.58	5.03	5.19			343.51	5.57	5.75	5.56	5.64
293.54	5.05	5.22	5.04	5.11	344.47	5.58	5.77		
294.55	5.06	5.22			345.58	5.59	5.78	5.59	5.67
295.56	5.07	5.24			351.65	5.66	5.84		
297.52	5.08	5.25			352.68	5.67	5.85		
298.53	5.09	5.26			353.68	5.68	5.87		
299.56	5.11	5.28			354.50	5.69	5.88		
300.52	5.10	5.28			362.46	5.78	5.97		
302.52	5.14	5.31			363.44	5.79	5.98	5.78	5.87
303.53	5.15	5.32	5.15	5.22	364.45	5.80	5.99	5.80	5.88
304.69	5.16	5.33	5.15	5.23	365.48	5.82	6.00		
305.54	5.17	5.34	5.17	5.24	367.49	5.84	6.03		
306.47	5.18	5.36	5.18	5.25	369.50	5.86	6.04		
307.48	5.20	5.37	5.19	5.26	370.47	5.87	6.06		
308.49	5.21	5.38			373.52	5.91	6.09	5.90	5.98
309.51	5.21	5.39	5.21	5.28	374.49	5.92	6.10	5.91	5.99
310.56	5.23	5.40	5.22	5.29	383.48	6.02	6.21		
312.76	5.24	5.42			385.47	6.04	6.22	6.03	6.11

On balance and given the present flux distribution the method likely to give the most realistic value is the integration under the spline fit to the $U-M$ data. The results from the other methods are given because it has not been possible to obtain M observations on all nights and general trends can be seen quite satisfactorily in the integrations of the $U-L$ data. Additionally a comparison of the spline and blackbody fits to a given dataset gives some indication of the uncertainty involved in the integration technique itself. Although we have continued to use blackbody fitting to the flux data we are not suggesting that the flux is in any way behaving as a blackbody over the time period discussed here. This approach is intended purely as an integration technique. The temperatures and radii derived from the blackbody fits are not tabulated here because they no longer appear physically meaningful.

The problems discussed earlier in this section largely affect the absolute measurement of the

Table 6. The e-folding times for the various magnitudes.

Band	Days since core collapse 147 to 265	265 to 385	Notes
U	2905 (340)	627 (21)	
B	145.6 (0.6)	160.9 (0.6)	
V	112.9 (0.3)	114.8 (0.2)	
R_c	133.7 (0.4)	106.8 (0.4)	
I_c	142.6 (0.6)	96.7 (0.5)	
J	87.4 (0.4)	85.9 (0.3)	
H	66.7 (0.2)	92.7 (0.6)	
K	[70.6 (0.3)]	[69.6 (0.2)]	
L	59.4 (0.2)	83.7 (0.8)	
M_{bol}	110.4 (0.6)	100.4 (0.3)	U to M spline
M_{bol}	114.7 (0.4)	101.4 (0.5)	U to M blackbody
M_{bol}	105.4 (0.3)	100.1 (0.2)	U to L spline
M_{bol}	114.9 (0.3)	101.9 (0.4)	U to L blackbody

total flux, as do uncertainties in the reddening (see Paper II). Because the spectrum of the supernova evolved very slowly with time there should be less uncertainty in measurements of trends such as the linear decline rate (Paper III) and the departure from it, which is discussed below.

6 Individual light curves

Although the light curves in various wavebands are of less theoretical interest than is the bolometric curve, they are potentially important for comparison with observations of other supernovae for which bolometric light curves have not been obtained. It is of particular interest to look at the behaviour in the individual bands over the period when the bolometric light curve was closely following the decay of ^{56}Co (Paper III). The individual light curves, with the exception of that for *K* (see below) all exhibit a change in slope during the period from days 240 to 270. The e-folding times for each of the bands determined between days 147 and 265 (the 'linear-decay' phase) and between days 265 and 385 (the 'post-linear-decay' phase) are given in Table 6. The numbers given in parentheses are the standard errors for the straight line fits. These times differ greatly from one colour to the next. The variation in the decline rate for different colours is a consequence of a change in relative flux distribution which is illustrated for two representative days in Fig. 6. In this figure the two flux distributions are normalized to their respective bolometric magnitudes. This means that colours, such as the *V* magnitude, which have declined at a rate close to that of the bolometric magnitude, will lie close on the 2 days while the *JHKL* colours, which have declined much faster than the bolometric rate, lie well below their earlier relative values by day 374. It is interesting that the *V* curve decay rate is so similar to that of the bolometric curve, indicating that a more or less constant bolometric correction ($BC = M_{bol} - V_0$) of -0.3 mag was applicable over the 'linear-decay' phase. The decay times for the *K* light are given in parentheses as they are slightly misleading in that *K* does not show an obvious change of slope near day 265. Instead it decayed with e-folding times of 75.2($\pm$0.5), 65.9($\pm$0.2) and 70.9($\pm$0.4) in the period between days 147 and 215, 215 and 300, and 300 and 385, respectively.

It is of interest to compare our results with those derived using the *IUE* fine error sensor (FES). During the period of linear decline when the bolometric curve (Paper III) had an e-folding time between 100 and 115 days, depending on the method of flux integration, the e-folding time of the FES magnitude was 136 days (Panagia 1987). The FES has a broad spectral response which peaks at about 4600 Å, falls rapidly into the ultraviolet and more slowly into the red (Holm & Crabb 1979). It essentially covers the same spectral range as do the $BV(RI)_c$ filters, with a heavy weighting on the region covered by the *B* band. Because of this wide spectral coverage the

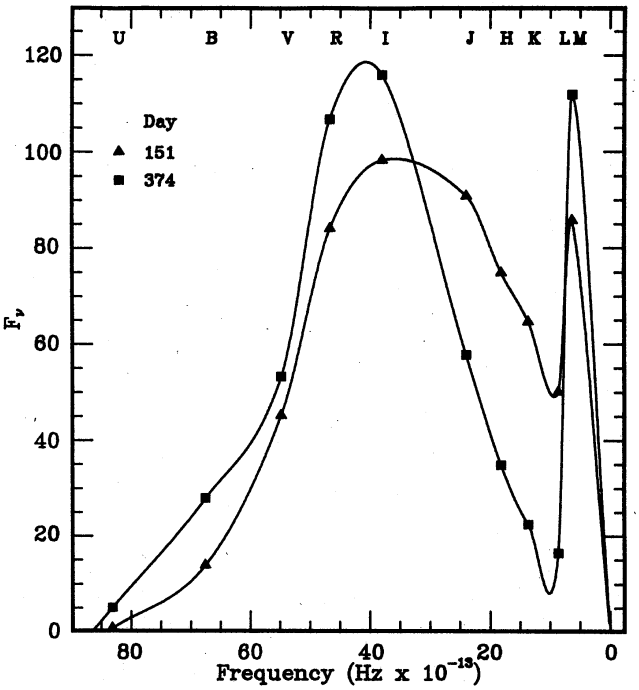

Figure 6. The flux distribution of SN 1987A on day 151 (triangles), at the beginning of the 'linear-decay' phase and on day 374 (squares) during the 'post-linear-decay' phase. The curves are normalized to give the same bolometric magnitude.

effective wavelength of the FES will change with the photometric development of the supernova. It is obvious from the decay rates given in Table 6 for the linear decay period (days 147–265) and from the flux distribution of the supernova in Fig. 6, that a filter with the characteristics of the FES will give a decay time appreciably longer than that of the bolometric magnitude. A similar conclusion has now been reached by Panagia (private communication). Determining the bolometric magnitude as we have done from photometry in several broadbands extending from the near ultraviolet to the near infrared unquestionably provides a much better estimate of the total flux than does a single band, even a relatively broad one, such as the FES.

7 The energy balance for SN 1987A

The two major sources of energy powering the light curve of SN 1987A are energy deposited in the outer envelope by the passage of the initial shock wave and that generated by the decay of ^{56}Ni and ^{56}Co. The total energy radiated by SN 1987A after 1.5 days following core collapse was calculated from the bolometric light curve (Papers I–IV) based on 0.35–5.0 μm (U–M) photometry. After day 265 a significant fraction of the ^{56}Co decay energy escaped as γ-rays (see Section 8), and we shall therefore discuss only the period up to that day. The flux radiated before day 1.5 was computed from the models given by Nomoto & Shigeyama (1987). This amounts to only about 1 per cent of the total flux of 9.1×10^{48} erg radiated up to day 265.

We have presented evidence here and elsewhere (Paper III) that the linear decline phase of SN 1987A was powered entirely by the radioactive decay of ^{56}Co, and fixed the initial mass of ^{56}Ni at 0.08 M_0. The radioactive decay of ^{56}Co and ^{56}Ni provided a total energy of 13.8×10^{48} by day 265. Thus there was a clear excess of production over radiation of energy. The discrepancy amounts to 6×10^{48} erg when account is taken of Woosley's (1988) theoretical prediction, that until about day 40 the radiation from SN 1987A was due to the release of energy deposited by the initial shock wave.

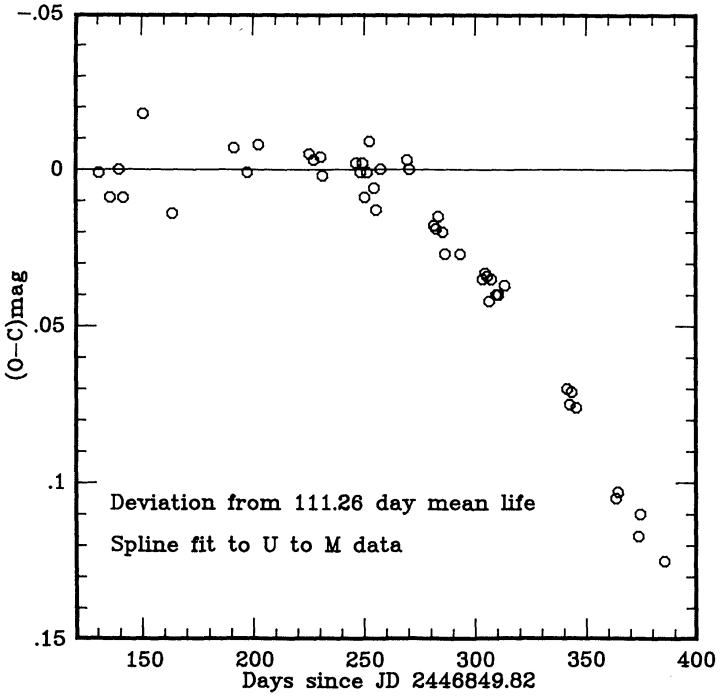

Figure 7. The residuals in bolometric magnitude from the straight line with the slope expected for radioactive decay of ^{56}Co. The bolometric magnitudes were determined by integrating under spline fits to the *U–M* data. The predicted magnitude (C) is found by fitting a straight line with slope 111.26 days to the observations between days 120 and 265. (O–C) is then the difference between the observed magnitudes (O) and the predictions.

Woosley (1988 and private communication) has pointed out that, after the explosion, the layers containing elements heavier than helium will typically move at 2000 km s^{-1} with a front-to-back range of only a few hundred km s^{-1}. The Co–Ni–Fe shell lies at the base of these layers and the dissipation of the excess decay energy, which is equivalent to about twice the kinetic energy of the mass 56 material, will significantly affect the dynamics of the overlying layers. According to Woosley a density inversion appears in the lower layers leading to an instability which results in ^{56}Co-rich material moving outwards and giving rise to the changes in the observed flux discussed below.

8 Discussion

In Paper III (also Feast 1987) we showed that the bolometric light curve of the supernova declined linearly from days 147 to 260. The e-folding time of the decline lay between 110 and 115 days depending on the technique used for flux integration. This provided the first direct evidence that the decline phase in this supernova is powered by the decay of ^{56}Co, which has a mean life of 111.3 days. This deduction has subsequently been supported by the detection both of Co II line emission (Rank *et al.* 1988) and of the 847 and 1238 keV lines (Matz *et al.* 1987) produced during the radioactive decay of ^{56}Co to ^{56}Fe.

The residuals from the fit of a straight line with a slope of 111.3 days to the bolometric light curve as a function of time are shown in Fig. 7. There is a clear deviation from the linear decline starting around day 265 and reaching the 10 per cent level at about day 360 in the *U–M* bolometric flux curve (see also Catchpole & Whitelock 1988). A similar result is obtained if the bolometric magnitudes determined from the more numerous *U* to *L* data are used. This deviation is in the sense that the light curve decays more rapidly than during the earlier linear phase and has an

e-folding time of 100 days between days 265 and 385. Taken at its face value this result suggests that the outer layers of the supernova have become at least partially optically thin to γ-rays from ^{56}Co. However, given the caveat in Section 5 on possible uncertainties in the bolometric flux determination, it is important to confirm this directly. In fact on day 340 the γ-ray and related X-ray flux from SN 1987A (Kumagai *et al.* 1988; Nomoto, private communication) was about 8 per cent of the total luminosity. Given the uncertainty on the high-energy flux measurements, this is exactly the flux required to make up the deficit in the photometrically determined light curve. Therefore the change in the slope of the bolometric light curve and the detection of compensating γ-rays together very strongly suggest that the decay of ^{56}Co continues to be the sole significant source of energy within the supernova in this period.

Early supernova models suggested that the outer layers should become optically thin to γ-rays only after about 2 yr. However, more recently, and particularly after the detection of the γ-radiation, it was suggested that some mixing may have occurred and that fingers of processed material could penetrate the outer layers (Ebisuzaki & Shibazaki 1988; Woosley 1988; Nomoto & Shigeyama 1987). Such a model would appear to explain the effects in evidence here.

The continued close agreement between the observed decline in the total flux and that expected from the decay of ^{56}Co indicates that there is still a negligible contribution to the bolometric flux from other possible energy sources such as a pulsar or a light echo.

Acknowledgments

We are indebted to Stan Woosley for useful comments regarding Section 7. We also thank Ken Nomoto for communicating various observations in advance of publication.

References

Catchpole, R. M. & Whitelock, P. A., 1988. *IAU Circ. No. 4544.*

Catchpole, R. M., *et al.*, 1987. *Mon. Not. R. astr. Soc.*, **229**, 15P (Paper II).

Catchpole, R. M., *et al.*, 1988. *Mon. Not. R. astr. Soc.*, **231**, 75P (Paper III).

Ebisuzaki, T. & Shibazaki, N., 1988. *Astrophys. J. Lett.*, submitted.

Feast, M. W., 1987. *Supernova 1987A in the Large Magellanic Cloud. 4th George Mason Fall Workshop in Astrophysics,* p. 51, eds M. Kafatos & A. Michalitsianos, Cambridge University.

Holm, A. V. & Crabb, W. G., 1979. *NASA IUE Newsletter no. 7,* 40.

Kumagai, S., Itoh, M., Shigeyama, T., Nomoto, K. & Nishimura, J., 1988. *Astr. Astrophys.*, in press.

Matz, S. M., Share, G. H., Leising, M. D., Chupp, E. L., Vestrand, W. T. & Beresford, A. C., 1987. *IAU Circ. No. 4510.*

Menzies, J. W., *et al.*, 1987. *Mon. Not. R. astr. Soc.*, **227**, 39P (Paper I).

Nomoto, K. & Shigeyama, T., 1987. *Supernova 1987A in the Large Magellanic Cloud. 4th George Mason Fall Workshop in Astrophysics,* Cambridge University, in press.

Oliva, E., Moorwood, A. F. M. & Danziger, I. J., 1987. *ESO Messenger No. 50,* 18.

Panagia, N., 1987. *Supernova 1987A in the Large Magellanic Cloud. 4th George Mason Fall Workshop in Astrophysics,* p. 96, eds M. Kafatos & A. Michalitsianos, Cambridge University.

Rank, D. M., Pinto, P. A., Woosley, S. E., Bregman, J. D., Witteborn, F., Axelrod, T. S. & Cohen, M., 1988. *Nature,* **331**, 505.

Woosley, S. E., 1988. *Astrophys. J.*, in press.

Woosley, S. E., Arnett, W. D. & Clayton, D. D., 1973. *Astrophys. J. Suppl.*, **26**, 231.

Young, L. A., 1968. *J. Quantit. Spectrosc. Radiat. Transfer,* **8**, 693.